Fabrication of a novel aluminum surface covered by numerous high-aspect-ratio anodic alumina nanofibers

Daiki Nakajima, Tatsuya Kikuchi*, Shungo Natsui, Norihito Sakaguchi, Ryosuke O. Suzuki
Faculty of Engineering, Hokkaido University
N13-W8, Kita-ku, Sapporo, Hokkaido, 060-8628, Japan

* Corresponding author: Tatsuya Kikuchi
TEL: +81-11-706-6340
FAX: +81-11-706-6342
E-mail: kiku@eng.hokudai.ac.jp

Abstract

The formation behavior of anodic alumina nanofibers via anodizing in a concentrated pyrophosphoric acid under various conditions was investigated using electrochemical measurements and SEM/TEM observations. Pyrophosphoric acid anodizing at 293 K resulted in the formation of numerous anodic alumina nanofibers on an aluminum substrate through a thin barrier oxide and honeycomb oxide with narrow walls. However, long-term anodizing led to the chemical dissolution of the alumina nanofibers. The density of the anodic alumina nanofibers decreased as the applied voltage increased in the 10 to 75 V range. However, active electrochemical dissolution of the aluminum substrate occurred at a higher voltage of 90 V.

Low temperature anodizing at 273 K resulted in the formation of long alumina nanofibers measuring several micrometers in length, even though a long processing time was required due to the low current density during the low temperature anodizing. In contrast, high temperature anodizing easily resulted in the formation and chemical dissolution of alumina nanofibers. The structural nanofeatures of the anodic alumina nanofibers were controlled by choosing of the appropriate electrochemical conditions, and numerous high-aspect-ratio alumina nanofibers (>100) can be successfully fabricated. The anodic alumina nanofibers consisted of a pure amorphous aluminum oxide without anions from the employed electrolyte.

Keywords: Aluminum; Anodizing; Anodic Alumina Nanofibers; Pyrophosphoric Acid

1. Introduction

Aluminum oxide films fabricated via anodizing in various electrolyte solutions have been widely investigated in various applied sciences and technologies due to their characteristic nanomorphologies and chemical/physical properties. In general, anodic aluminum oxide can be classified into two different types as follows: barrier and porous oxides [1-3]. Aluminum anodizing in neutral solutions results in the formation of a thin dense barrier oxide that can be as thick as 1 μm on the aluminum substrate [4,5]. Barrier oxides have been widely used for electrolytic capacitor applications due to their high dielectric property [6-8]. In contrast, aluminum anodizing in acidic solutions including inorganic, carboxylic, cyclic oxocarbonic, and bisphosphonate acid results in the formation of porous oxide that can be as thick as several hundred μm [9-16]. Porous oxides possess numerous fine hexagonal unit cells that have a nanoscale pore in the center [1-3]. Notably, the hexagonal cells of the porous oxide are self-ordered during anodizing when aluminum is anodized in the appropriate acidic electrolyte solutions under the appropriate electrochemical conditions, and highly ordered porous oxides with an ideal cell arrangement can be easily fabricated [17,18]. For self-ordering of the porous alumina, several appropriate acidic electrolytes (i.e., sulfuric (H_2SO_4) [19,20], selenic (H_2SeO_4) [21,22], oxalic (HOOC-COOH) [23-25], malonic (HOOC-CH_2-COOH) [26-28], phosphoric (H_3PO_4) [18,29,30], tartaric (HOOC-$(CHOH)_2$-COOH) [27], phosphonoacetic ($(HO)_2P(O)CH_2COOH$)) [31], and etidronic ($CH_3C(OH)[PO(OH)_2]_2$) acid [32,33]) have been previously reported. In addition, additional acidic electrolytes and the use of organic solvents have also been reported by several research groups for novel porous alumina with different nanomorphologies [34-39]. Anodic oxide including nanoparticles were successfully fabricated by anodizing using sputter coated aluminum alloys and oxide nanoparticle dispersion aluminum [40,41]. Anodic porous alumina has been widely used for various nanoapplications, such as optical devices and nanotemplates [42-51].

The electrolyte used in aluminum anodizing has important effects on the nanofeatures of the anodic oxide. Therefore, the discovery of an additional electrolyte would lead to the formation of different types of anodic oxides with unique nanofeatures. Very recently, we reported the fabrication of a novel anodic aluminum oxide, which was called “anodic alumina nanofibers”, by anodizing in a new electrolyte (i.e., pyrophosphoric acid ($H_2P_2O_7$)) [52]. Ultra-high density single nanometer-scale alumina nanofibers measuring approximately 10^{14} m^{-2} in density are formed on the aluminum substrate during pyrophosphoric acid anodizing. These novel nanofeatures are very different from that obtained by typical anodizing for barrier and porous oxides, as previously described. In addition, the aluminum surface that is covered with anodic alumina nanofibers exhibited superhydrophilic behavior with a contact angle of less than 1° within 1 second. This novel third generation anodic oxide can be used for various nanoapplications, such as a catalyst support and wettability control due to their ultralarge surface area. However, the details of the growth behavior of the anodic alumina nanofibers during pyrophosphoric acid anodizing under different experimental conditions, such as voltages, temperatures, and anodizing times, remain unclear. Therefore, detailed investigations of the pyrophosphoric acid anodizing are required for understanding the formation of alumina nanofibers and how to control the nanomorphology.

In the current investigation, we studied the formation behavior of the anodic alumina nanofibers via constant voltage pyrophosphoric acid anodizing under various conditions using high-resolution scanning electron microscopy (SEM) and transmission electron microscopy (TEM). We determined that there are appropriate pyrophosphoric acid anodizing conditions, such as time, temperature, and applied voltage, for the formation of uniform anodic alumina nanofibers. We found that the length, density, and nanomorphology of the anodic alumina nanofibers could be accurately controlled by the electrochemical operating conditions. Moreover, we found that numerous high-aspect-ratio anodic alumina nanofibers (>100) connected to the aluminum substrate can be fabricated via long-term pyrophosphoric acid anodizing at low temperature of 273 K. These novel alumina nanofibers fabricated via pyrophosphoric acid anodizing will contribute to improving the functional surface materials.

2. Experimental

High-purity aluminum foils and plates (99.99 wt%, 20 mm × 20 mm with a handle, 110 μm thick from Showa Aluminum, Japan, 400 μm thick from Nippon Light Metal, Japan) were used as the anodizing specimens. The aluminum specimens were ultrasonically degreased in an ethanol solution for 10 min, and then, a silicone resin was coated on the bottom of the handle. After drying the coated silicone resin, the specimens were electropolished in a 13.6 M CH_3COOH/2.56 M $HClO_4$ mixture (T = 280 K) at a constant voltage of 28 V for 1 min. An aluminum plate was used as a cathode for electropolishing. Then, the specimens were washed with distilled water and dried.

The electropolished specimens were immersed in a concentrated pyrophosphoric acid solution (74.0-78.0 wt%, 100 cm^3, T = 273-313 K, Kanto Chemical, Japan), and then, the samples were anodized at a constant voltage at 10 to 95 V for up to 72 h using a PC-connected direct-current power supply (PWR-400H, Kikusui, Japan). The electrolyte solutions were slowly stirred (1 s^{-1}) with a magnetic stirrer during anodizing and maintained at a constant temperature using a water bath (UCT-1000, AS ONE, Japan). A platinum plate was used as the cathode for pyrophosphoric acid anodizing. The corresponding current during the constant voltage anodizing was recorded by a digital multi-meter (DMM4040, Tektronix, USA). After pyrophosphoric acid anodizing, the specimens were washed with distilled water and dried in a desiccator.

The surface nanomorphology of the anodized specimens was examined by field emission SEM (JIB-4600F/HKD and JSM-6500F, JEOL, Japan) and TEM (Titan Cubed G2 60-300, FEI, USA). For the SEM observations, a thin platinum conductive layer was coated on the specimens by a sputter coater (MSP-1S, Vacuum Device, Japan). The density of the anodic alumina nanofibers was calculated by the SEM observation of the lower honeycomb structures. For the TEM observations, the specimens were embedded in an epoxy resin, trimmed mechanically, and then sliced into thin sections using an ultramicrotome (PT-X POWERTOME, Boeckler, USA) with a diamond knife. Qualitative analysis of the incorporated anions in the anodic oxide was performed using energy-filtered TEM (EFTEM) and electron energy-loss spectroscopy (EELS).

3. Results and discussion

3.1 Typical formation behavior of anodic alumina nanofibers

To understand the formation behavior of the anodic alumina nanofibers, the

electropolished aluminum specimens were anodized in pyrophosphoric acid under various experimental conditions, such as applied voltages, temperatures, and times. Fig. 1 shows the electrochemical results and the changes in the current density, j, with anodizing time, t, at different constant voltages, U, during pyrophosphoric acid anodizing (T = 293 K). At a low voltage of 10 V, the current density increases and decreases rapidly to approximately 6 Am^{-2} immediately after the voltage was applied. Then, the current density decreases gradually with the anodizing time through a slight up-and-down variation for 5-10 min. The current density at other voltages during the initial 10 min increases with anodizing voltage, and key peaks were observed for 15 min at 25 V, 7 min at 50 V, and 3 min at 75 V. The position of the peak shifts with anodizing voltage toward the initial stage of anodizing. In contrast, the current densities become nearly the same values of approximately 2-3 Am^{-2} for longer periods of anodizing. These current-time transients and peak shifts were very similar to that obtained by typical anodizing for anodic porous alumina [1]. However, the current density increases rapidly to over 2500 Am^{-2} in the very initial stage at 90 V, and active anodic dissolution of the aluminum substrate was observed during anodizing. High-voltage anodizing above 95 V at different temperatures in the range of 273-313 K resulted in similar active dissolution of the aluminum substrate. Therefore, the application of a high voltage in concentrated pyrophosphoric acid is inappropriate for the formation of anodic oxide on aluminum. The changes in the surface nanomorphology under each of the anodizing conditions were examined by SEM.

Fig. 2 shows the SEM images of the specimen anodized in pyrophosphoric acid at 50 V and 293 K that was measured in Fig. 1. Periodic stripe patterns that were approximately 90 nm in length were observed on the electropolished aluminum specimen as a starting material (Fig. 2a). In general, these stripe patterns were formed on the electropolished aluminum surface, and these patterns have also been reported in several previous studies [53]. Here, a thin native oxide film including a very small amount of chloride ions that are a few nanometers in thickness was formed on the aluminum substrate after electropolishing in the $HClO_4/CH_3COOH$ solution [54]. Similar periodic strip patterns were also observed on the surface anodized for 30 s (Fig. 2b). However, the thin barrier anodic oxide, which was several tens of nanometers in thickness, was observed on the aluminum substrate by SEM observation of the fracture cross-section. This thin barrier oxide was immediately formed on the aluminum substrate by applying a constant voltage.

When the anodizing time increased to 2 min (Fig. 2c), the shape of the patterns on the anodic oxide clearly shifts to a porous pattern from the stripe pattern. Due to additional anodizing for 4 min (Fig. 2d), a honeycomb oxide structure with narrow hexagonal walls was formed on the aluminum specimen. Based on a high-magnification fracture cross-section observation, the anodic oxide consists of two layers including a bottom barrier oxide and an upper honeycomb oxide. Although the nanomorphology of the oxide is very similar to the structure of anodic porous alumina [2], the nanopores in the honeycomb layer are considerably larger than those obtained by typical anodizing in other acidic solutions [2]. Therefore, vigorous chemical dissolution of the anodic oxide occurs during the porous layer formation.

Further anodizing for 10 min (Fig. 2e) results in the formation of characteristic three-dimensional nanostructures that are different from the anodic porous alumina.

Although the narrow hexagonal walls dissolve into the solution, only the rod-shaped oxide located at the apices of the honeycomb structures remains at this stage. The development of alumina nanofibers at the apices began immediately after the formation of the honeycomb structures. The thickness of the bottom barrier oxide remained unchanged as the anodizing time increased (compared with Figs. 2d and 2e). This behavior is very similar to that of the barrier oxide during the growth of the anodic porous alumina. When the anodizing time increased to 12 min (Fig. 2f), the alumina nanofibers increased in length to several hundred nanometers, and several nanofibers became tangled and bundled together due to bending under their own weight. These bundles may be structured by the surface tension and adsorption of each nanofiber via drying of distilled water on the surface after specimen washing [55]. After anodizing for 30 min (Fig. 2g), large-scale nanofiber bundles were formed on the honeycomb structures due to additional growth of alumina nanofibers. The density of the anodic alumina nanofibers was measured to be 1.6×10^{14} m^2 by SEM observation.

Although the anodic alumina nanofibers can be successfully fabricated via pyrophosphoric acid anodizing at 50 V and 293 K, as described in Fig. 2, long-term anodizing leads to the extinction of the alumina nanofibers formed on the aluminum specimen. Fig. 3 shows the SEM images of the anodic alumina nanofibers formed via further pyrophosphoric acid anodizing for a) 60 min and b) 360 min. The large bundles, which consist of many longer alumina nanofibers, were observed on the aluminum specimen after 60 min (Fig. 3a). However, extremely narrow and feeble alumina nanofibers were formed via long-term anodizing for 360 min (Fig. 3b), and several nanofibers peeled off from the apices of the honeycomb structures. Anodic alumina nanofibers can be chemically dissolve via long-term immersion in a concentrated pyrophosphoric acid. In addition, the current density decreases with the anodizing time (Fig. 1), and the growth rate of the alumina nanofibers also decreased with the anodizing time. Therefore, feeble alumina nanofibers were observed on the aluminum specimen due to long-term pyrophosphoric acid anodizing. However, this long-term anodizing may be the best approach for the fabrication of extremely narrow anodic alumina nanofibers. As the aluminum specimen was anodized in a 50 vol% diluted pyrophosphoric acid solution, typical anodic porous alumina was formed on the aluminum substrate. However, anodic alumina nanofiber could not be observed on the anodic oxide.

In Fig. 1, the position of the peak shifted with anodizing voltage toward the initial stage. During constant voltage anodizing in typical acidic electrolyte solutions, the peak corresponds to the formation and growth of the nanopores in the anodic oxide. As the applied voltage is high, rapid formation of the pores was induced. Because similar growth behavior may occur in the initial stage of pyrophosphoric acid anodizing, the time before the appearance of the peak current density decreased with anodizing voltage increased.

In summary, the anodic alumina nanofibers are formed on the aluminum specimen via barrier and honeycomb layer formations using pyrophosphoric acid anodizing. This three-step nanofiber formation including the generation of the barrier, honeycomb, and fibrous oxides was also observed for all of the pyrophosphoric acid anodizing cases, as discussed in the next section.

3.2 Anodic alumina nanofibers fabricated via anodizing under various conditions

Fig. 4 shows the surface morphologies of the specimen anodized in pyrophosphoric acid (T = 293 K) for 60 min at different voltages (i.e., U = a) 75 V, b) 25 V, and c) 10 V). At 75 V (Fig. 4a), anodic alumina nanofibers grown at the apices of the lower honeycomb structures were observed, which is similar to that shown in Fig. 2g. The density of the anodic alumina nanofibers was measured to be 1.1×10^{14} m^2, which is less than that at 50 V (1.6×10^{14} m^2). As the anodizing voltage decreased to 25 V (Fig. 4b), the average diameter of the lower honeycomb structure decreased. In general, this decreased density was observed in the cell diameter (interpore distance) for the fabrication of anodic porous alumina. Therefore, the density of alumina nanofibers increased and was measured to be 2.7×10^{14} m^2. These experimental results suggest that the density of the anodic alumina nanofibers can be easily controlled by the applied voltage during pyrophosphoric acid anodizing. However, irregular-shaped alumina nanofibers with bonding structures were observed at extremely low voltage anodizing (i.e., U = 10 V, Fig. 4c) due to the distance between each apex on the honeycomb structure being too close. Therefore, appropriate applied voltages for the fabrication of anodic alumina nanofibers were determined to be 25-75 V at 293 K.

Because nanofibers grow at the apices of the lower honeycomb structures, the density of the nanofibers depends on the density of the lower honeycomb structures. During constant voltage anodizing in typical acidic electrolyte solutions, the cell diameter of the honeycomb structures increases with applied voltage. In pyrophosphoric acid anodizing, a similar relationship was observed in Fig. 4. Therefore, the density of the nanofibers increases with applied voltage decreases during pyrophosphoric acid anodizing.

The nanomorphology of the anodic alumina nanofibers fabricated by pyrophosphoric acid anodizing also strongly depends on the acid temperature. Fig. 5 shows the changes in the current density with anodizing time during pyrophosphoric acid anodizing at U = 50 V and different temperatures (i.e., T = 273-313 K). At a low temperature of 273 K, an extremely low current density (i.e., approximately 0.5 Am^{-2}) was measured during anodizing after the initial period. The current densities for the steady-state anodizing increase with the pyrophosphoric acid temperature. Therefore, even if the same voltage was applied to the aluminum specimens during pyrophosphoric acid anodizing, the growth rate and morphology of the anodic oxide may be different at each anodizing temperature. The position of the peak shifted with temperature toward the initial stage, because the growth rate of the anodic oxide increased with temperature.

Fig. 6 shows the SEM images of the aluminum specimens anodized at 50 V and various temperatures of 273-313 K for 60 min, as described in Fig. 5. At T = 273 K, stripe/honeycomb intermediate anodic oxides are formed on the aluminum surface that are similar to the nanostructures shown in Figs. 2c and 2d. At this temperature, the anodic alumina nanofiber was not observed on the surface due to the extremely low current density during pyrophosphoric acid anodizing at 273 K. As the temperature increased to 283 K (Fig. 6b), the bundles, which consisted of anodic alumina nanofibers, were observed on the honeycomb oxide layer due to the sufficient current density and corresponding growth behavior. However, the length of each alumina nanofiber was shorter than that obtained at 293 K (Fig. 3a). At 303 K (Fig. 6c), irregular-shaped anodic alumina nanofibers possessing different lengths and diameters were observed on

the aluminum surface. This nanofeature is very similar to that obtained via long-term anodizing for 360 min at 293 K under the same voltage condition (Fig. 3b). In addition, this nanofeature is formed by the chemical dissolution of the anodic oxide in pyrophosphoric acid at high temperatures. A further increase in the temperature results in the formation of oxide debris on the aluminum specimen due to active dissolution of the anodic oxide (Fig. 6d). Therefore, pyrophosphoric acid anodizing at high temperatures is not suitable for the fabrication of long alumina nanofibers.

The results shown in Fig. 6a indicated that anodic alumina nanofibers were not formed on the aluminum specimen by pyrophosphoric acid anodizing at a low temperature of 273 K for 1 h. However, the honeycomb anodic oxide observed in Fig. 6a was extremely similar to that obtained via anodizing at 293 K for 4 min, as shown in Fig. 2d. Therefore, further long-term anodizing at 273 K may also result in the formation of anodic alumina nanofibers. Fig. 7 shows the change in the current density with anodizing time during pyrophosphoric acid anodizing at U = 50 V and T = 273 K for t = 72 h. The current density showed a steady value of approximately 0.4 Am^{-2} after the initial transient period, although there are several small oscillations during ling-term anodizing. Therefore, the steady-state growth of the alumina nanofibers will be occurred under this anodizing condition. Fig. 8 shows the SEM images of the aluminum surface anodized via pyrophosphoric acid anodizing at 50 V and 273 K for a) t = 6 h, b) 24 h, and c) 72 h. As the anodizing time increased to 6 h (Fig. 8a) from 1 h (Fig. 6a), the aluminum surface became covered with numerous anodic alumina nanofibers. The length of the alumina nanofibers increased with the anodizing time (Figs. 8b and 8c), and bundles, which consisted of alumina nanofibers that were several micrometers in length, were formed on the specimen. The diameter of the alumina nanofibers was measured as approximately 11 nm via the high-resolution SEM images. However, note that the nanofibers were covered by a thin platinum electroconductive layer for the SEM observations. The aspect ratio of each alumina nanofiber was calculated to be above 100 from the SEM observation. The fabrication of novel high-aspect-ratio anodic alumina nanofibers can be achieved via long-term pyrophosphoric acid anodizing at low temperatures due to the low solubility of the alumina nanofibers. These high-aspect-ratio nanofibers are useful for the catalyst support and wettability control with ultralarge surface area.

As shown in Fig. 6, high temperature anodizing for 60 min results in the complete extinction of the anodic alumina nanofibers via chemical dissolution. In addition, alumina nanofibers were formed under the same anodizing conditions for a short time period. Fig. 9 shows the SEM image of the aluminum specimen anodized by pyrophosphoric acid at 50 V and 313 K for a short anodizing time of 10 min. Although the length and width of the alumina nanofibers were irregular due to active dissolution at high temperatures, alumina nanofibers were observed on the anodized specimen after 10 min. Therefore, high temperature anodizing is appropriate for the rapid fabrication of anodic alumina nanofibers with a disordered shape. This rapid fabrication is important for providing superhydrophilic properties on the aluminum surface [52].

Pyrophosphoric acid anodizing of aluminum proceeds by the successive formation of the barrier, honeycomb, and fibrous oxide layers, and the structural nanofeatures of the anodic alumina nanofibers can be controlled by adjusting the operating conditions, such as the applied voltage, temperature, and time. Therefore, a

novel aluminum surface covered with well-defined anodic alumina nanofibers can be fabricated via accurately controlled pyrophosphoric acid anodizing. Very recently, we successfully fabricated high-density highly ordered anodic alumina nanofibers on an aluminum surface using these insights [56]. In contrast, the anodic alumina nanofibers completely dissolve by the pyrophosphoric acid during long-term anodizing, and this behavior is primarily determined by the acid temperature.

3.3 TEM observations of the anodic alumina nanofibers

In a previous study, we reported that anodic alumina nanofibers fabricated by pyrophosphoric acid anodizing consisted of pure aluminum oxide based on TEM analysis [52]. In this TEM observation, the specimen was prepared by mechanical removal of the anodic alumina nanofibers from the surface. Therefore, clear elemental mapping of the cross-sectional anodized specimen was not obtained. In the current investigation, the anodized specimens were sliced using an ultramicrotome to observe the nanofeatures and measure the elemental distributions of the anodic oxide by TEM.

Fig. 10 shows the TEM image (left) and corresponding EFTEM elemental mapping images (right) of the aluminum specimen anodized via pyrophosphoric acid anodizing at 50 V and 293 K for 10 min, as shown in Fig. 2e. During this anodizing period, the anodic alumina nanofibers were generated at the apices of the honeycomb structures by the dissolution of the narrow oxide walls. In the TEM image, the bottom layer corresponds to the crystalline aluminum substrate, and the upper portions correspond to the amorphous anodic oxide (see the insert diffraction pattern). The corresponding elemental mapping images indicate that the anodic oxides contain phosphorous due to the pyrophosphate anion. Typically, anodic oxide prepared by anodizing to form barrier and porous oxides also contains anions of the employed electrolyte. However, phosphorous is not distributed in the long and narrow center portions of the anodic oxide, as indicated by the yellow arrows. Phosphorous was nonuniformly distributed in the anodic oxide formed by pyrophosphoric acid anodizing.

Fig. 11 shows the TEM image (upper left), corresponding EFTEM elemental mapping images (upper right), and EELS spectra (lower) of the aluminum specimen anodized via long-term anodizing for 30 min, as shown in Fig. 2g. In the TEM image, amorphous anodic alumina nanofibers measuring approximately 12-16 nm in width were observed on the bottom honeycomb oxide. Based on a comparison of the elemental distributions, the anodic alumina nanofibers consist of pure aluminum oxide without phosphorous. In contrast, the bottom honeycomb oxide contains anions of the electrolyte used. Similar analysis results regarding the uneven distribution of phosphorous were also obtained from the EELS spectra (P-$L_{2,3}$ edge). As the aluminum specimen is anodized in the pyrophosphoric acid solution, amorphous aluminum oxide with anions was formed on the aluminum substrate, and pure aluminum oxide without anions was also formed at the apices of the honeycomb structure. Although most of the bottom honeycomb oxide can be easily chemically dissolved into the concentrated pyrophosphoric acid during anodizing due to their impure composition, only the pure aluminum oxide remains on the surface in this condition. Therefore, amorphous pure anodic alumina nanofibers were formed via pyrophosphoric acid anodizing. However, long-term anodizing at high temperatures gradually results in the chemical dissolution of pure aluminum oxide, and the anodic alumina nanofibers are removed from the

surface, as shown in Fig. 6d.

4. Conclusions

This paper described the formation behavior of anodic alumina nanofibers fabricated via pyrophosphoric acid anodizing under various experimental conditions, such as applied voltages, temperatures, and times. Aluminum anodizing in concentrated pyrophosphoric acid results in the formation of anodic alumina nanofibers through barrier and honeycomb oxides. However, long-term anodizing leads to the chemical dissolution and extinction of the anodic alumina nanofibers. The density of the alumina nanofibers decreases as the applied voltage increases. However, anodizing at much lower ($U < 10$ V) and higher ($U > 90$ V) voltages and 293 K results in the formation of irregular-shaped alumina nanofibers and active dissolution of aluminum substrate, respectively. The growth rate of the alumina nanofibers increases with the temperature of the pyrophosphoric acid, and high temperature anodizing leads to the rapid dissolution of anodic oxide in the acid. Numerous high-aspect-ratio alumina nanofibers (>100) can be successfully fabricated via the appropriate electrochemical conditions. The anodic alumina nanofibers consist of amorphous pure aluminum oxide without anions that remain on the surface during pyrophosphoric acid anodizing due to their low dissolution rate. In summary, pyrophosphoric acid anodizing provided various characteristic nanofeatures on the aluminum surface.

Acknowledgments

This study was conducted at Hokkaido University and was supported by the "Nanotechnology Platform" Program of the Ministry of Education, Culture, Sports, Science, and Technology (MEXT), Japan. The authors wish to thank Prof. Hiroki Habazaki and Mr. Yuki Nakayama (Hokkaido University) for their assistance in the preparation of the TEM specimens. The work was financially supported by the Japan Society for the Promotion of Science (JSPS) "KAKENHI (24686080)", Toyota Physical & Chemical Research Institute Scholars, and the Light Metal Educational Foundation.

References

1) G.E. Thompson, Porous anodic alumina: fabrication, characterization and applications, Thin Solid Films 297 (1997) 192–201.
2) W. Lee, S.-J. Park, Porous anodic aluminum oxide: anodization and templated synthesis of functional nanostructures, Chem. Rev. 114 (2014) 7487–7556.
3) G.D. Sulka, Highly ordered anodic porous alumina formation by self-organized anodizing, in: A. Eftekhari (Ed.), Nanostructured Materials in Electrochemistry, Wiley-VCH, 2008, pp. 1–116.
4) Y. Li, H. Shimada, M. Sakairi, K. Shigyo, H. Takahashi, M. Seo, Formation and breakdown of anodic oxide films on aluminum in bolic acid/borate solutions, J. Electrochem. Soc. 144 (1997) 866–876.
5) K. Shimizu, H. Habazaki, P. Skeldon, G.E. Thompson, K. Marcus, Radio frequency glow discharge optical emission spectroscopy, Spectroscopy 17 (2002) 14–23.
6) H. Uchi, T. Kanno, R.S. Alwitt, Structural features of crystalline anodic alumina films, J. Electrochem. Soc. 148 (2001) B17–B23.
7) K. Watanabe, M. Sakairi, H. Takahashi, S. Hirai, S. Yamaguchi, Formation of Al–Zr

composite oxide films on aluminum by sol–gel coating and anodizing, J. Electroanal. Chem. 473 (1999) 250–255.
8) K. Watanabe, M. Sakairi, H. Takahashi, K. Takahiro, S. Nagata, S. Hirai, Anodizing of aluminum coated with silicon oxide by a sol-gel method, J. Electrochem. Soc. 148 (2001) B473–B481.
9) F. Keller, M.S. Hunter, D.L. Robinson, Structural Features of Oxide Coatings on Aluminum, J. Electrochem. Soc. 100 (1953) 411–419.
10) G.E. Thompson, G.C. Wood, Porous anodic film formation on aluminium, Nature 290 (1981) 230–232.
11) T. Kikuchi, T. Yamamoto, and R.O. Suzuki, Growth Behavior of Anodic Porous Alumina Formed in Malic Acid Solution, Appl. Surf. Sci. 284 (2013) 907–913.
12) T. Kikuchi, O. Nishinaga, S. Natsui, R.O. Suzuki, Fabrication of anodic porous alumina via acetylenedicarboxylic acid anodizing, ECS Electrochem. Lett. 3 (2014) C25–C28.
13) T. Kikuchi, T. Yamamoto, S. Natsui, R.O. Suzuki, Fabrication of Anodic Porous Alumina by Squaric Acid Anodizing, Electrochim. Acta 123 (2014) 14–22.
14) T. Kikuchi, D. Nakajima, J. Kawashima, S. Natsui, R.O. Suzuki, Fabrication of anodic porous alumina via anodizing in cyclicoxocarbon acids, Appl. Surf. Sci. 313 (2014) 276–285.
15) D. Nakajima, T. Kikuchi, S. Natsui, R.O. Suzuki, Growth behavior of anodic oxide formed by aluminum anodizing in glutaric and its derivative acid electrolytes, Appl. Surf. Sci. 321 (2014) 364–370.
16) W.J. Stępniowski, M. Norek, M. Michalska-Domańska, A. Bombalska, A. Nowak-Stępniowska, M. Kwaśny, Z. Bojar, Fabrication of anodic aluminum oxide with incorporated chromate ions, Appl. Surf. Sci. 259 (2012) 324–330.
17) A-P. Li, F. Müller, A. Birner, K. Nielsh, U. Gösele, Polycrystalline nanopore arrays with hexagonal ordering on aluminum, J. Vac. Sci. Technol. A 17 (1999) 1428–1431.
18) H. Masuda, K. Yada, A. Osaka, Self-ordering of cell configuration of anodic porous alumina with large-size pores in phosphoric acid solution, Jpn. J. Appl. Phys. 37 (1998) L1340–L1342.
19) S.Z. Chu, K. Wada, S. Inoue, M. Isogai, A. Yasumori, Fabrication of ideally ordered nanoporous alumina films and integrated alumina nanotubule arrays by high-field anodization, Adv. Mater. 17 (2005) 2115–2119.
20) G.D. Sulka, S. Stroobants, V. Moshchalkov, G. Borghs, J.P. Celis, Synthesis of well-ordered nanopores by anodizing aluminum foils in sulfuric acid, J. Electrochem. Soc. 149 (2002) D97–D103.
21) O. Nishinaga, T. Kikuchi, S. Natsui, R.O. Suzuki, Rapid fabrication of self-ordered porous alumina with 10-/sub-10-nm-scale nanostructures by selenic acid anodizing, Sci. Rep. 3 (2013) 2748.
22) T. Kikuchi, O. Nishinaga, S. Natsui, R.O. Suzuki, Self-ordering behavior of anodic porous alumina via selenic acid anodizing, Electrochim. Acta 137 (2014) 728–735.
23) O. Jessensky, F. Müller, U. Gösele, Self-organized formation of hexagonal pore arrays in anodic alumina, Appl. Phys. Lett. 72 (1998) 1173–1175.
24) L. Zaraska, W.J. Stępniowski, M. Jaskuła, G.D. Sulka, Analysis of nanopore arrangement of porous alumina layers formed by anodizing in oxalic acid at

relatively high temperatures, Appl. Surf. Sci. 305 (2014) 650–657.
25) W. Lee, R. Ji, U. Gösele, K. Nielsch, Fast fabrication of long-range ordered porous alumina membranes by hard anodization, Nat. Mater. 5 (2006) 741–747.
26) W. Lee, K. Nielsch, U. Gösele, Self-ordering behavior of nanoporous anodic aluminum oxide (AAO) in malonic acid anodization, Nanotechnology 18 (2007) 475713.
27) S. Ono, M. Saito, H. Asoh, Self-ordering of anodic porous alumina formed in organic acid electrolytes, Electrochim. Acta 51 (2005) 827–833.
28) G. Knörnschild, A.A. Poznyak, A.G. Karoza, A. Mozalev, Effect of the anodization conditions on the growth and volume expansion of porous alumina films in malonic acid electrolyte, Surf. Coat. Technol. doi:10.1016/j.surfcoat.2015.04.030
29) A-P. Li, F. Müller, A. Birner, K. Nielsh, U. Gösele, Hexagonal pore arrays with a 50–420 nm interpore distance formed by self-organization in anodic alumina, J. Appl. Phys. 84 (1998) 6023–6026.
30) J. Martín, C.V. Manzano, M. Martín-González, In-depth study of self-ordered porous alumina in the 140–400 nm pore diameter range, Micropor. Mesopor. Mat. 151 (2012) 311–316.
31) A. Takenaga, T. Kikuchi, S. Natsui, R.O. Suzuki, Self-ordered aluminum anodizing in phosphonoacetic acid and its structural coloration, ECS Solid State Lett. 4 (2015) P55–P58.
32) T. Kikuchi, O. Nishinaga, S. Natsui, R.O. Suzuki, Fabrication of self-ordered porous alumina via etidronic acid anodizing and structural color generation from submicrometer-scale dimple array, Electrochim. Acta 156 (2015) 235–243.
33) T. Kikuchi, O. Nishinaga, S. Natsui, R.O. Suzuki, Polymer nanoimprinting using an anodized aluminum mold for structural coloration, Appl. Surf. Sci. 341 (2015) 19–27.
34) M. Pashchanka, J.J. Schneider, Experimental validation of the novel theory explaining self-organizaition in porous anodic alumina films, Phys. Chem. Chem. Phys. 15 (2013) 7070–7074.
35) X. Qin, J. Zhang, X. Meng, C. Deng, L. Zhang, G. Ding, H. Zeng, X. Xu, Preparation and analysis of anodic aluminum oxide films with continuously tunable interpore distances, Appl. Surf. Sci. 328 (2015) 459–465.
36) T.-T. Kao, Y.-C. Chang, Influence of anodization parameters on the volume expansion of anodic aluminum oxide formed in mixed solution of phosphoric and oxalic acids, Appl. Surf. Sci. 288 (2014) 654–659.
37) M.A. Kashi, A. Ramazani, M. Rahmandoust, M. Noormohammadi, The effect of pH and composition of sulfuric-oxalic acid mixture on the self-ordering configuration of high porosity alumina nanohole arrays, J. Phys. D: Appl. Phys. 40 (2007) 4625–4630.
38) A. Zahariev, I. Kanazirski, A. Girginov, Anodic alumina films formed in sulfamic acid solution, Inorg. Chim. Acta 361 (2008) 1789–1792.
39) Q. Lin, B. Hua, S. F. Leung, X. Duan, Z. Fan, Efficient light absorption with integrated nanopillar/nanowell arrays for three-dimensional thin-film photovoltaic applications, ACS Nano 3 (2013) 2725–2732.
40) W. Chen, J.-S Wu, X.-H. Xia, Porous anodic alumina with continuously manipulated pore/cell size, ACS Nano 2 (2008) 959–965.

41) V.C. Gudla, F. Jensen, A. Simar, R. Shabadi, R. Ambat, Friction stir processed Al–TiO_2 surface composites: Anodising behaviour and optical appearance, Appl. Surf. Sci. 324 (2015) 554–562.
42) S.Z. Kure-Chu, K. Osaka, H. Yashiro, H. Segawa, K. Wada, S. Inoue, Controllable fabrication of networked three-dimensional nanoporous anodic alumina films on low-purity Al materials, J. Electrochem. Soc. 162 (2015) C24–C34.
43) A.P. Leontiev, O.A. Brylev, K.S. Napolskii, Arrays of rhodium nanowires based on anodic alumina: preparation and electrocatalytic activity for nitrate reduction, Electrochim. Acta 155 (2015) 466–473.
44) C.-W. Chu, Y.-C. Huang, C.-C. Tsai, J.-T. Chen, Wetting in nanopores of cylindrical anodic aluminum oxide templates: production of gradient polymer nanorod arrays on large-area curved surfaces, Eur. Polym. J. 63 (2015) 141–148.
45) T. Yanagishita, K. Nishio, H. Masuda, Anti-reflection structures on lenses by nanoimprinting using ordered anodic porous alumina, Appl. Phys. Express 2 (2009) 022001.
46) T. Yanagishita, M. Masui, N. Ikegawa, H. Masuda, Fabrication of polymer antireflection structures by injection molding using ordered anodic porous alumina mold, J. Vac. Sci. Technol. B 32 (2014) 021809.
47) T. Yanagishita, K. Nishio, H. Masuda, Two-dimensional photonic crystal composed of ordered polymer nanopillar arrays with high aspect ratios using anodic porous alumina templates, Appl. Phys. Express 1 (2008) 012002.
48) W. Lee, K. Schwirn, M. Steinhart, E. Pippel, R. Scholz, U. Gösele, Structural engineering of nanoporous anodic aluminium oxide by pulse anodization of aluminium, Nat. Nanotechnol. 3 (2008) 234–239.
49) S.Z. Chu, S. Inoue, K. Wada, D. Li, H. Haneda, S. Awatsu, Highly porous (TiO_2-SiO_2-TeO_2)/Al_2O_3/TiO_2 composite nanostructures on glass with enhanced photocatalysis fabricated by anodization and sol-gel process, J. Phys. Chem. B 107 (2003) 6586–6589.
50) T. Kumeria, M.M. Rahman, A. Santos, J. F.-Borrull, L.F. Marsal, D. Losic, Structure and optical nanoengineering of nanoporous anodic alumina rugate filters for real-time and label-free biosensing applications, Anal. Chem. 86 (2014) 1837–1844.
51) Y. Wang, A. Santos, G. Kaur, A. Evdokiou, D. Losic, Structurally engineering anodic alumina nanotubes as nano-carriers for delivery of anticancer therapeutics, Biomaterials 35 (2014) 5517–5526.
52) T. Kikuchi, O. Nishinaga, D. Nakajima, J. Kawashima, S. Natsui, N. Sakaguchi, R.O. Suzuki, Ultla-high density single nanometer-scale anodic alumina nanofibers fabricated by pyrophosphoric acid anodizing, Sci. Rep. 4 (2014) 7411.
53) V.V. Konovalov, G. Zangari, R.M. Metzger, Highly ordered nanotopographies on electropolished aluminum single crystals, Chem. Mater. 11 (1999) 1949–1951.
54) H. Takahashi, M. Nagayama, Surface films formed on aluminum by different pretreatments. I. XPS analysis of thickness and chemical composition, J. Mater. Finish Soc. Jpn. 36 (1985) 96–103.
55) J.-G. Fan, Y.-P. Zhao, Freezing a water droplet on an aligned Si nanorod array substrate, Nanotechnology 19 (2008) 155707.
56) D. Nakajima, T. Kikuchi, S. Natsui, R.O. Suzuki, Highly ordered anodic alumina

nanofibers fabricated via two distinct anodizing processes, ECS Electrochem. Lett. 4 (2015) H14–H17.

Captions

Fig. 1. Changes in the current density, j, as a function of anodizing time, t, during anodizing in concentrated pyrophosphoric acid at 293 K and constant voltages ranging from 10-90 V.

Fig. 2. SEM images of the aluminum specimens anodized in pyrophosphoric acid at 293 K and a constant voltage of 50 V for a) 0 through g) 30 min. The bottom rows show high magnification SEM images of the fracture surface for 30 s, 4 min, 10 min, and 12 min.

Fig. 3. SEM images of the aluminum specimens anodized in pyrophosphoric acid at 293 K and a constant voltage of 50 V for a) 60 min and b) 360 min.

Fig. 4. SEM images of the aluminum specimens anodized in pyrophosphoric acid at 293 K and different constant voltages of a) 75 V, b) 25 V, and c) 10 V for 60 min.

Fig. 5. Changes in the current density, j, as a function of anodizing time, t, during anodizing in pyrophosphoric acid at 273-313 K and a constant voltage of 50 V.

Fig. 6. SEM images of the aluminum specimens anodized in pyrophosphoric acid at a) 273 K, b) 283 K, c) 303 K, and d) 313 K and a constant voltage of 50 V for 60 min.

Fig. 7. Change in the current density, j, as a function of anodizing time, t, during anodizing in pyrophosphoric acid at 273 K and 50 V for long-term of 72 h.

Fig. 8. SEM images of the anodic alumina nanofibers formed via long-term pyrophosphoric acid anodizing at 273 K and a constant voltage of 50 V for a) 6 h, b) 24 h, and c) 72 h.

Fig. 9. SEM images of the anodic alumina nanofibers formed via short-term pyrophosphoric acid anodizing at 313 K and a constant voltage of 50 V for 10 min.

Fig. 10. TEM image, diffraction pattern, and corresponding EFTEM elemental distribution mapping images of the aluminum specimen anodized in pyrophosphoric acid at 293 K and a constant voltage of 50 V for 10 min.

Fig. 11. TEM image, diffraction pattern, corresponding EFTEM elemental distribution mapping images, and EELS spectra of the aluminum specimen anodized in pyrophosphoric acid at 293 K and a constant voltage of 50 V for 30 min.

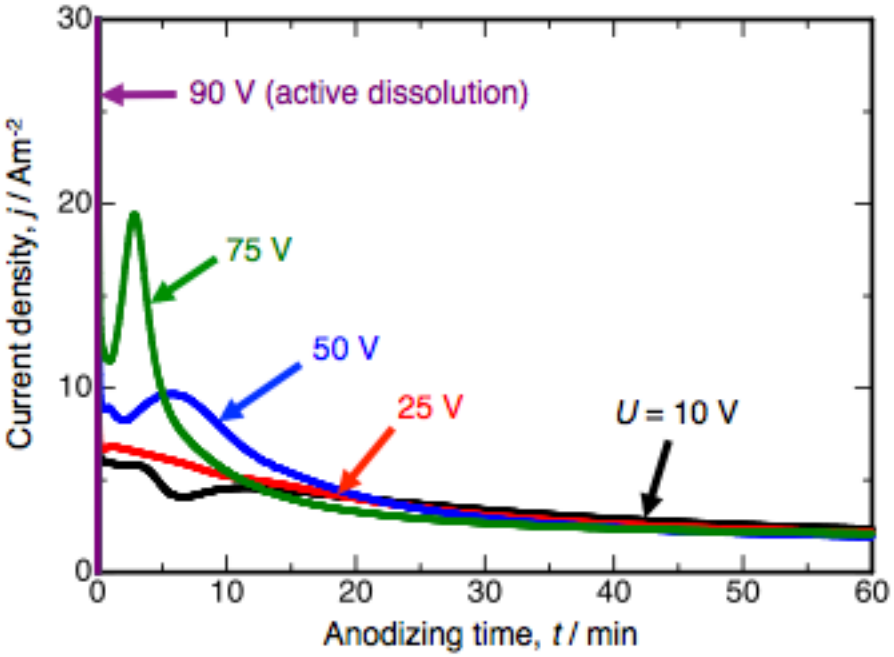
90 V (active dissolution)
75 V
50 V
25 V
U = 10 V
Current density, j / Am-2
Anodizing time, t / min
0
10
20
30
40
50
60

Fig. 1

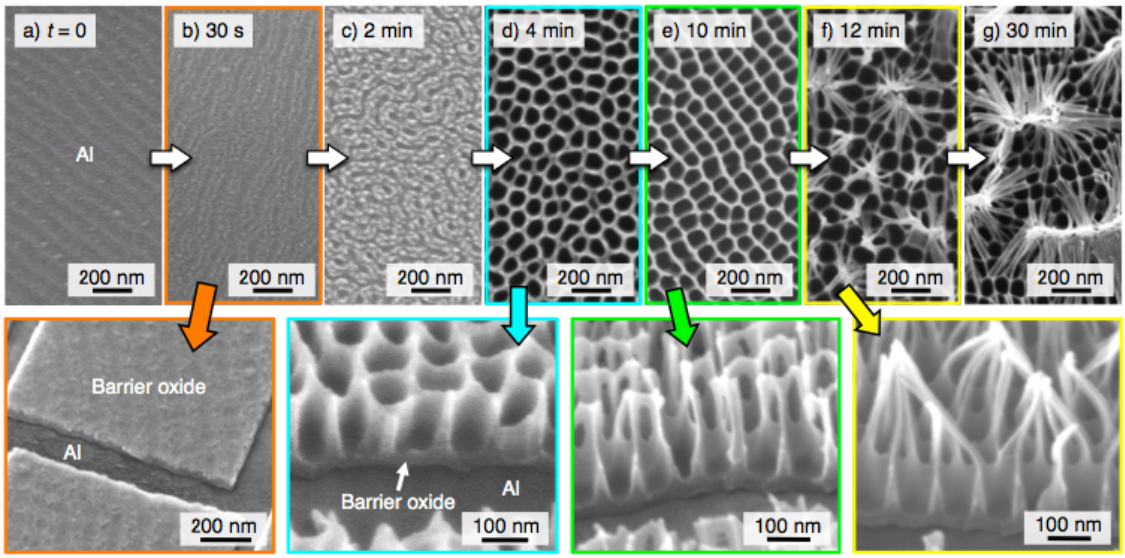
a) t = 0
Al
200 nm
b) 30 s
200 nm
c) 2 min
200 nm
d) 4 min
200 nm
e) 10 min
200 nm
f) 12 min
200 nm
g) 30 min
200 nm
Barrier oxide
Al
200 nm
Barrier oxide
Al
100 nm
100 nm
100 nm

Fig. 2

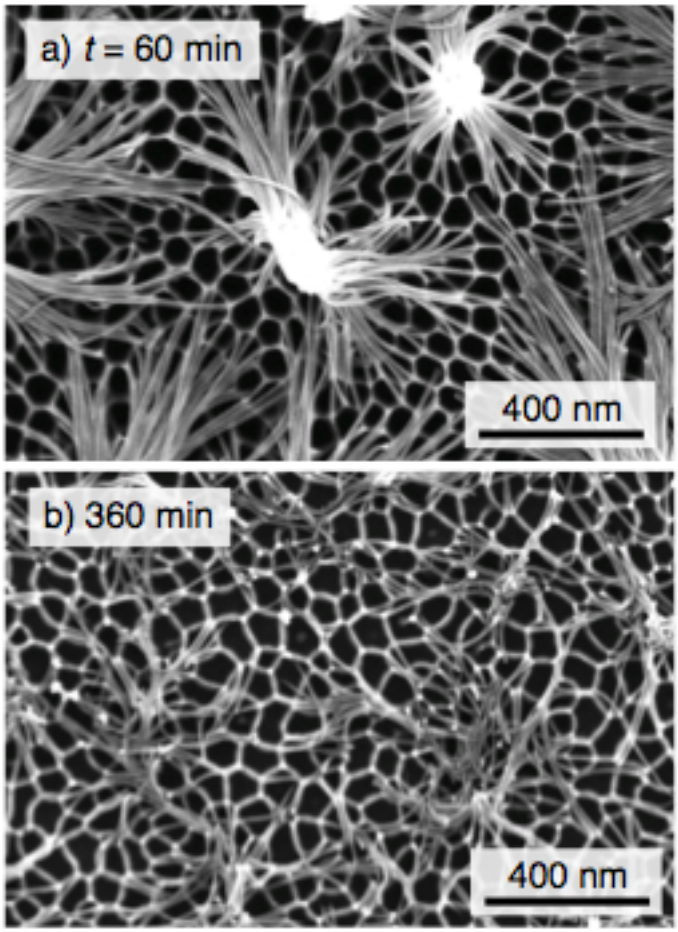

Fig. 3

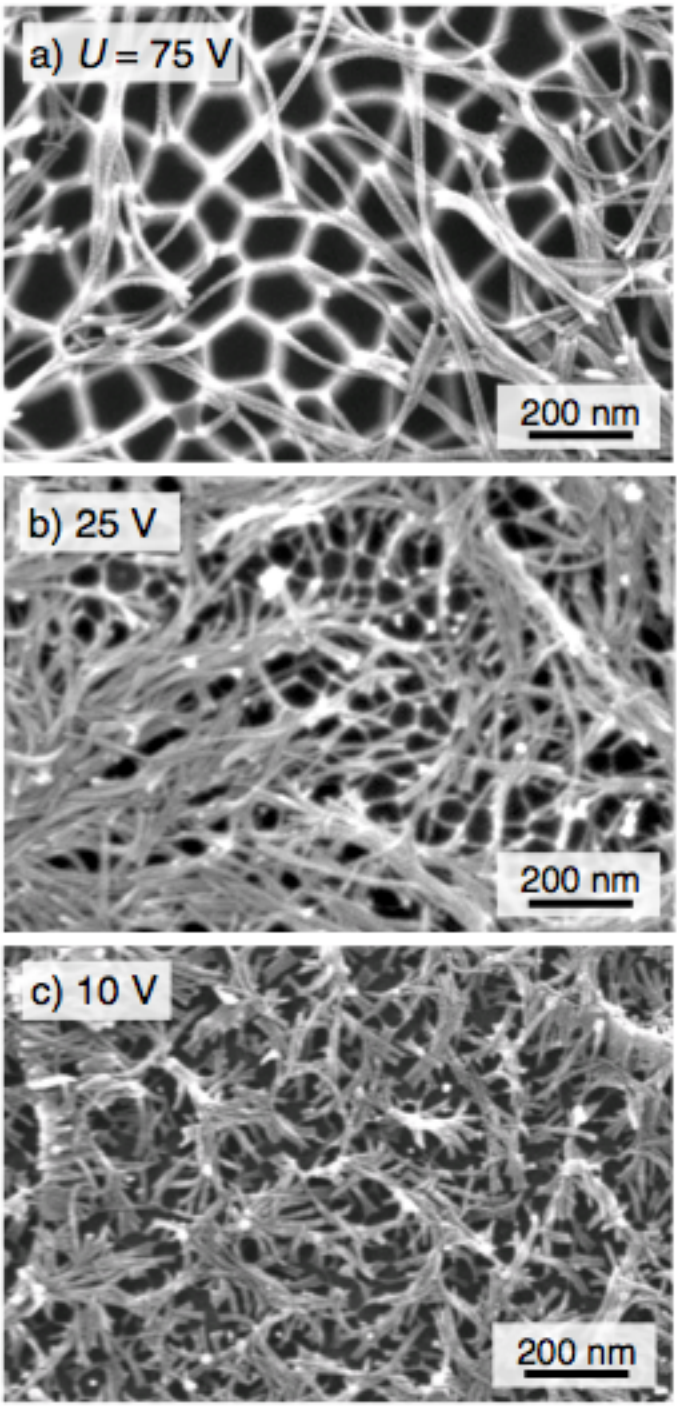

Fig. 4

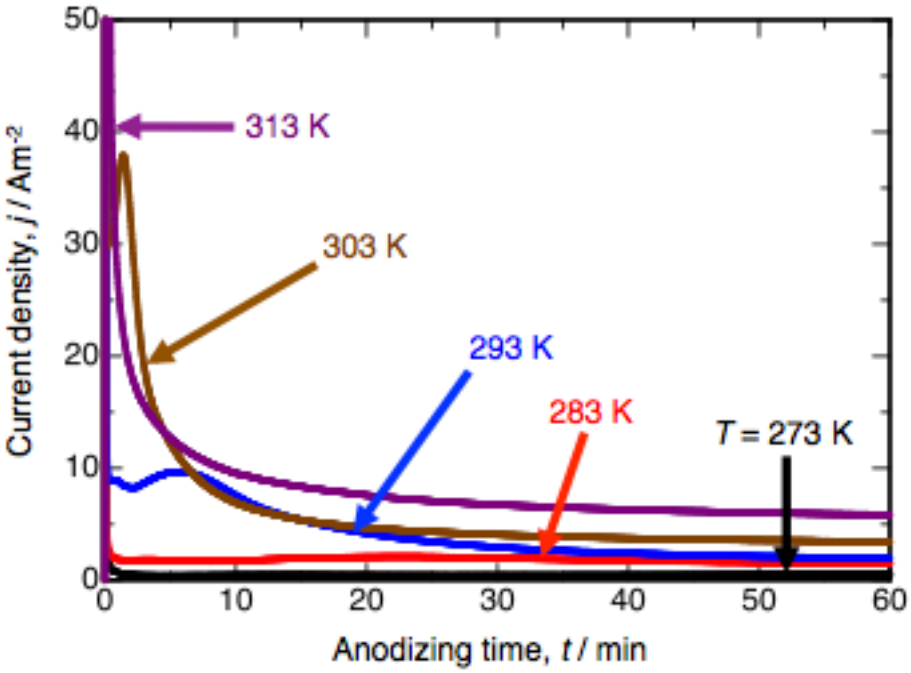
Current density, j / Am-2
Anodizing time, t / min
313 K
303 K
293 K
283 K
T = 273 K
0
10
20
30
40
50
60

Fig. 5

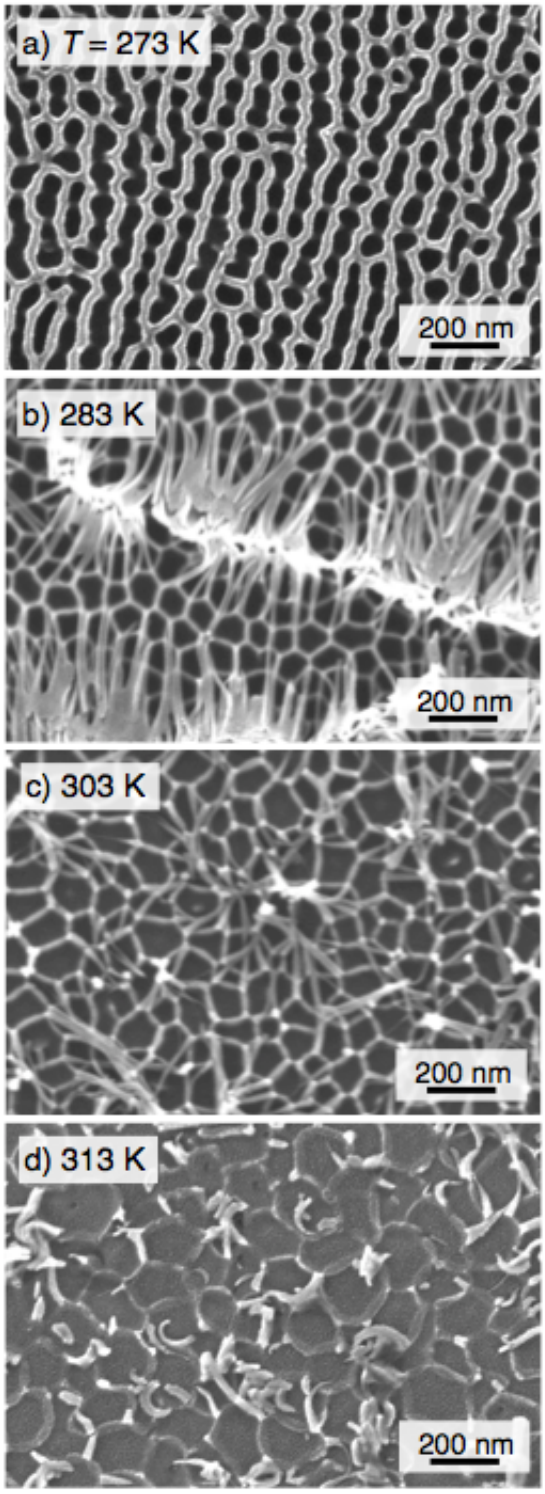

Fig. 6

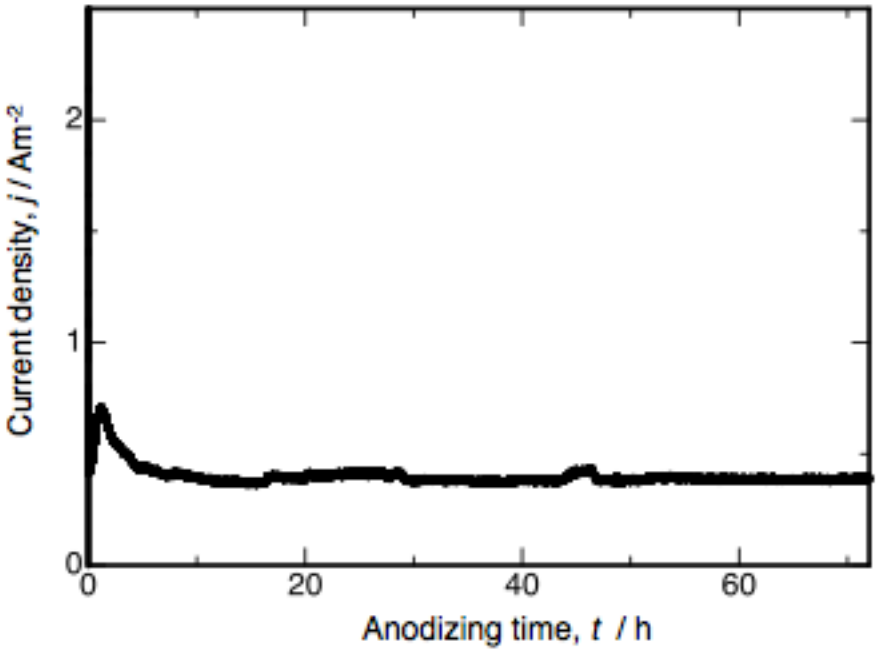

Fig. 7

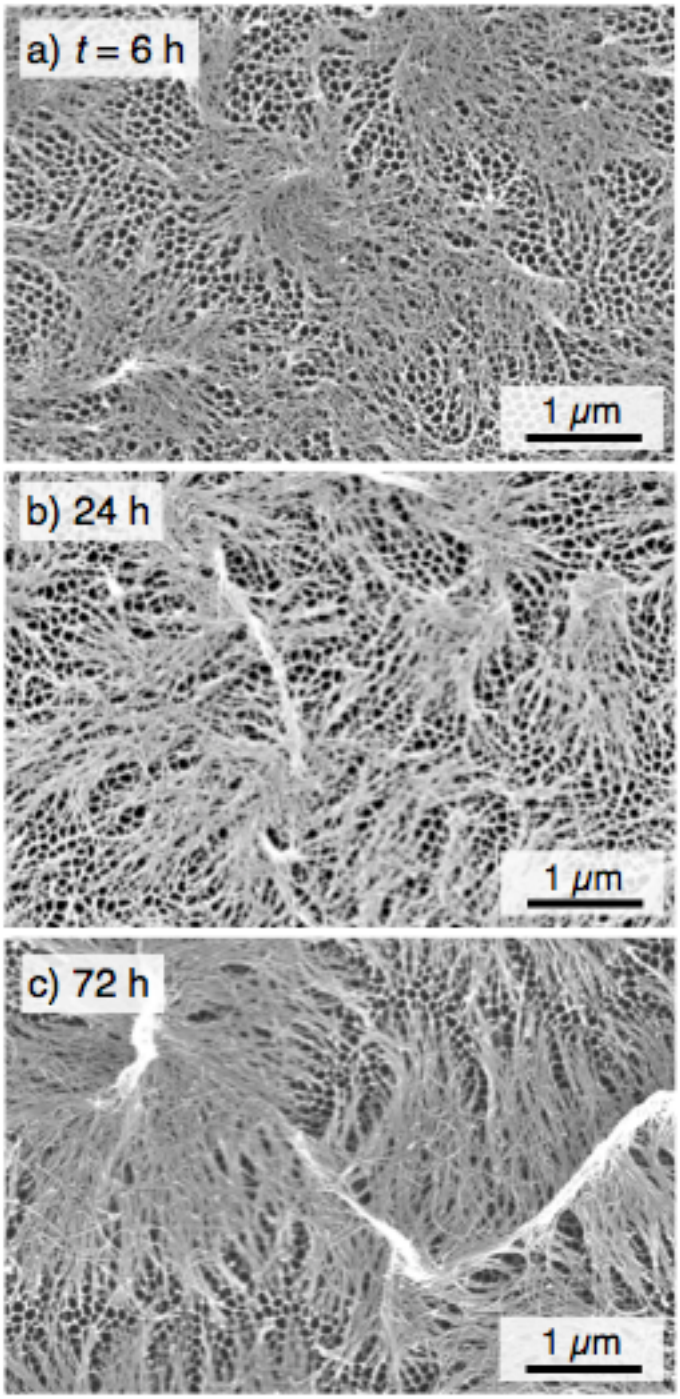

Fig. 8

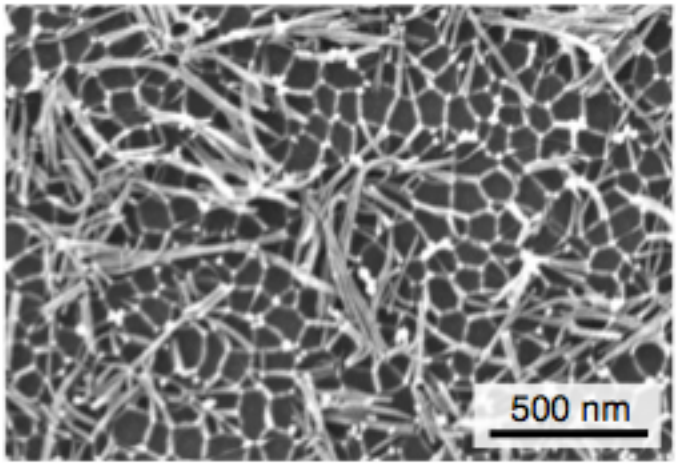

Fig. 9

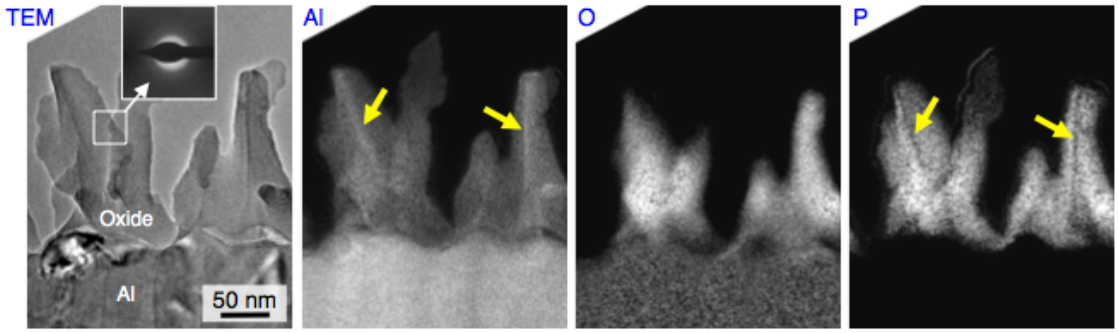

Fig. 10

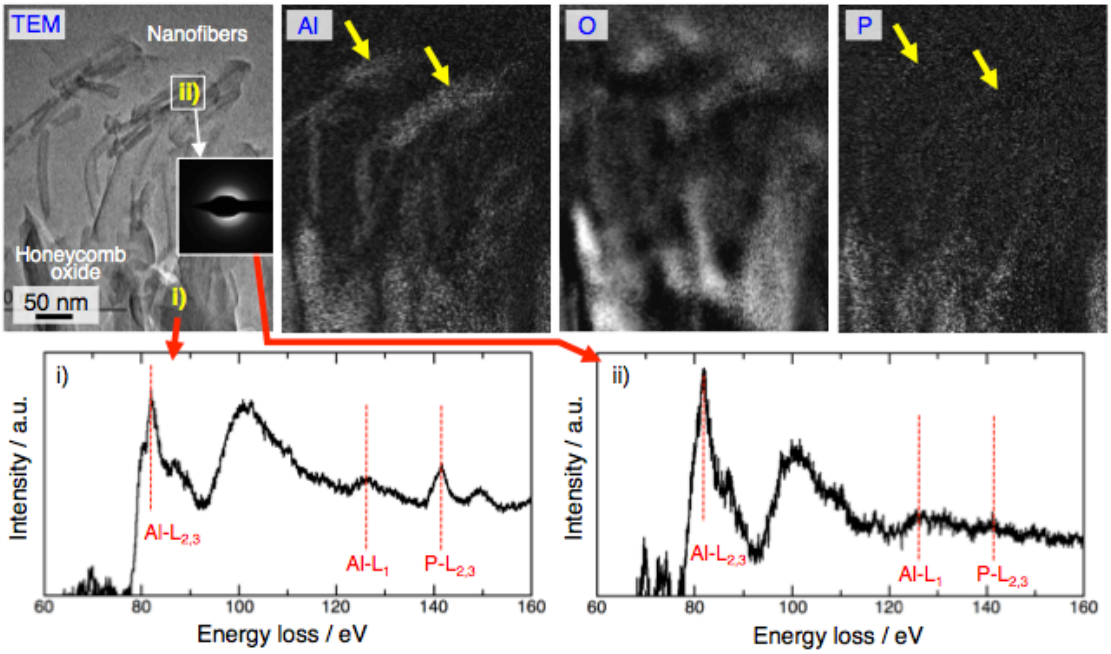
TEM
Nanofibers
ii)
Honeycomb oxide
50 nm
i)
Al
O
P
i)
Intensity / a.u.
Al-L2,3
Al-L1
P-L2,3
60
80
100
120
140
160
Energy loss / eV
ii)
Intensity / a.u.
Al-L2,3
Al-L1
P-L2,3
60
80
100
120
140
160
Energy loss / eV

Fig. 11